New Journal of Physics
The open access journal at the forefront of physics

Deutsche Physikalische Gesellschaft DPG
IOP Institute of Physics

Published in partnership with: Deutsche Physikalische Gesellschaft and the Institute of Physics

OPEN ACCESS

RECEIVED
29 September 2014

REVISED
14 December 2014

ACCEPTED FOR PUBLICATION
9 January 2015

PUBLISHED
4 February 2015

PAPER

Model Hamiltonian for topological Kondo insulator SmB_6

Rui Yu[1], **Hongming Weng**[2,3], **Xiao Hu**[1], **Zhong Fang**[2,3] **and Xi Dai**[2,3]

[1] International Center for Materials Nanoarchitectonics (WPI-MANA), National Institute for Materials Science, Tsukuba 305-0044, Japan
[2] Beijing National Laboratory for Condensed Matter Physics, and Institute of Physics, Chinese Academy of Sciences, Beijing 100190, People's Republic of China
[3] Collaborative Innovation Center of Quantum Matter, Beijing 100190, People's Republic of China

E-mail: Hu.Xiao@nims.go.jp **and** daix@aphy.iphy.ac.cn

Keywords: topological Kondo insulator, surface states, spin texture

Abstract

Starting from the k·p method in combination with first-principles calculations, we systematically derive the effective Hamiltonians that capture the low energy quasi-particle structures of the recently discovered topological Kondo insulator SmB_6. Using these effective Hamiltonians we can obtain both the energy dispersion and the spin texture of the topological surface states, which can be detected by further experiments.

1. Introduction

Searching for new topological insulators (TIs) has become an active research field in condensed matter physics [1, 2]. A topological insulator has an insulating and topologically non-trivial bulk band structure giving rise to robust Dirac like surface states, which are protected by time reversal symmetry and have the spin-momentum locking feature. Such topological surface states have several remarkable properties, for example, the suppression of back scattering and localization on the TI's surface [3–7]. Furthermore, if superconductivity is induced on the surface of TIs via proximity effects, Majorana bound states can be induced [8–10]. These novel properties make TIs a promising platform for the design of spintronics devices and future quantum computing applications [11].

Recently the mixed valence compound SmB_6 has been proposed to be a TI and attracts lots of research interest [12–18]. Unlike the other well studied TIs, i.e. the Bi_2Se_3 family of materials, the strong correlation effects in mixed valence TIs are crucial in understanding electronic structure owing to the partially filled 4f bands [18–20]. There are two main effects induced by the on-site Coulomb interaction among the 4f-electrons: one is the strong modification of the 4f band width, the other is the correction to the effective spin–orbit coupling and crystal field [21–23]. As a consequence, the band inversion in the modified band structure happens between the 5d and 4f band (with total angular momentum $j = 5/2$) around three X points in the Brillouin zone (BZ). In the Bi_2Se_3 family of materials, the band inversion happens between two bands both with the p character and similar band width. The situation in SmB_6 is quite different, where the band inversion happens between 5d and 4f bands with the band widths differing by orders of magnitude, which leads to very unique low energy electronic structure. The band inversion happens at the BZ boundary (X points), which projects to three different points in the surface BZ leading to three different Dirac points on generic surfaces.

Experimentally, the first evidence of topological surface states was found by transport measurements, and then by angle-resolved photoemission spectroscopy (ARPES), scanning tunneling spectroscopy (STS) and quantum oscillation magneto-resistance measurements [24–36]. Unlike the electronic structures in the large energy scale, which is mainly determined by the local atomic physics, the topological nature of the electronic structure can be fully described by the quasi-particle structure only, whose form can be determined from the symmetry principles. In the present paper, we will construct a k·p model capturing the full topological and symmetry features of the low energy quasi-particle structure, which leads to topological surface states with the renormalized Fermi velocities. All the symmetry allowed terms in the above k·p model have been obtained by fitting with the band structure obtained from the LDA+Gutzwiller calculations introduced in a previous paper

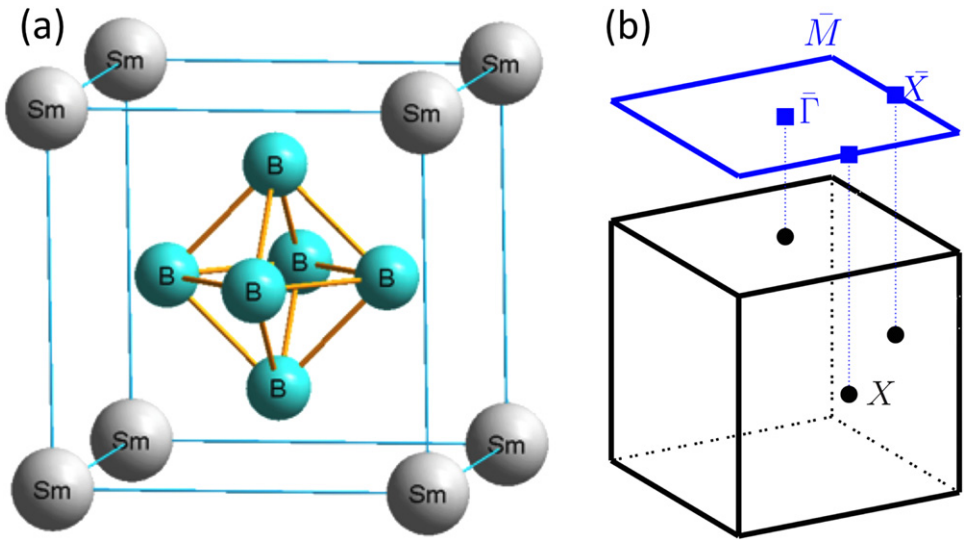

Figure 1. (a) The CsCl-type structure of SmB_6 with a $Pm\bar{3}m$ space group. Sm ions and B_6 octahedron are located at the corner and center of the cubic lattice respectively. (b) The bulk BZ of SmB_6 (black cubic) and its projection onto the (001) direction (blue square). The X points (black dots) in the bulk BZ are projected to $\bar{\Gamma}$ and $\bar{X}$ points (blue square points) in the (001) surface BZ.

[18]. Such an analytical model gives a clear theoretical description for the quasi-particle structure of SmB_6, which can be widely used in further studies.

The organization of the present paper is as follows. In section 2, we present the crystal and band structures of SmB_6. Then we construct the effective model to describe the bulk band structure of this material from symmetry considerations in section 3. Furthermore we calculate surface states and the spin texture on the (001) surface based on our model Hamiltonian and show that it is consistent with the tight-binding calculation results. In section 4, we calculate the quasi-particle interference on the SmB_6 (111) surface based on our surface model Hamiltonians. Conclusions are given at the end of this paper.

2. Crystal structure and calculated electronic band structure of SmB_6

In this section we first describe the crystal structure of SmB_6 and then discuss its nontrivial topological bulk band structure.

2.1. Crystal structure

SmB_6 has a CsCl-type crystal structure with a $Pm\bar{3}m$ space group. The Sm ions are located at the corner and the B_6 octahedron is located at the body center of the cubic lattice as shown in figure 1(a). The bulk BZ and the surface BZ in the (001) direction are shown in figure 1(b).

2.2. Electronic structure

previous electronic structure studies found that in SmB_6 the band inversion happens between Sm 4f bands with total angular momentum $j = 5/2$ and one of the 5d bands, which leads to fractional occupation in 4f $j = 5/2$ orbitals or 'non-integer chemical valence' [37–40]. Since the band inversion happens at three X points in the BZ, where the 4f and 5d states have opposite parities, the Z_2 topologically non-trivial band structure is formed [41, 42].

In order to include the strong Coulomb interaction among the f electrons, we implement the local density approximation (LDA) in density functional theory with the Gutzwiller variational method (LDA+Gutzwiller) and apply it to calculate the renormalized band structure of SmB_6.

Here we briefly introduce the LDA+Gutzwiller method. For detailed descriptions please refer to [18, 43]. The LDA+Gutzwiller method combines the LDA with Gutzwiller variational method, which takes care of the strong atomic feature of the f-orbitals in the ground state wave function. In this method, we implement the single particle Hamiltonian obtained by LDA with on-site interaction terms describing the atomic multiplet features, which can be written as,

$$H = H_{\mathrm{LDA}} + H_{\mathrm{int}} + H_{\mathrm{DC}} \tag{1}$$

where $H_{\rm LDA}$, $H_{\rm int}$ and $H_{\rm DC}$ represent the LDA Hamiltonian, on-site interaction and the double counting term respectively [44]. The LDA Hamiltonian can be expressed in a tight-binding form by constructing the projected Wannier functions for both 5 d and 4f bands [45–47]. The on-site interactions can be described in terms of Slater integrals as introduced in detail in the previous paper [18]. The double counting term $H_{\rm DC}$ subtracts the correlation energy that is already included in LDA calculations. Within the Gutzwiller approximation, an effective Hamiltonian $H_{\rm eff}$ describing the quasi-particle band structure can be obtained, which describes the low energy dynamics including the topological surface states [18]. To further study the low energy physics of SmB_6, i.e. the behavior of the surface states, a simple k·p model Hamiltonian will be very useful. In the next section, we will construct such a model by expanding $H_{\rm eff}$ near the three X points.

3. Model Hamiltonian for SmB_6

3.1. Model Hamiltonian for bulk states at X points

In this section, we will systematically derive the effective Hamiltonian near X points based on k·p theory combined with the results of first-principles calculations. We only give the effective Hamiltonian at the $X_1 = (0, 0, \frac{1}{2})$ point. The effective Hamiltonians at the other two X points can be obtained by acting C_{4x} or C_{4y} rotation operations to the Hamiltonian at X_1. Using the symmetry group at the X point we can construct the effective k·p model near this point and all the parameters used in such a model can be obtained by fitting to the renormalized band structure obtained by the LDA+Gutzwiller method.

The k·p Hamiltonian is obtained from our one-partial effective Hamiltonian

$$H_{\rm eff}\psi_{n,\mathbf{k}}(\mathbf{r}) = E_{n,\mathbf{k}}\psi_{n,\mathbf{k}}(\mathbf{r}), \tag{2}$$

where $\psi_{n,\mathbf{k}} = e^{i\mathbf{k}\cdot\mathbf{r}}u_{n,\mathbf{k}}(\mathbf{r})$ are the Bloch wave functions and the effective Hamiltonian consists of kinetic-energy operator, local periodic crystal potential and the spin–orbit interaction term:

$$H_{\rm eff} = \frac{p^2}{2m} + V(\mathbf{r}) + \frac{\hbar}{4m^2c^2}(\boldsymbol{\sigma}\times\nabla V)\cdot\mathbf{p}. \tag{3}$$

In terms of the cellular functions $u_{n,\mathbf{k}}(\mathbf{r})$, equation (2) becomes

$$H_{\mathbf{k}}u_{n,\mathbf{k}}(\mathbf{r}) \equiv \left[\frac{p^2}{2m} + V(\mathbf{r}) + \frac{\hbar}{4m^2c^2}(\sigma\times\nabla V)\cdot(\mathbf{p}+\hbar\mathbf{k}) + \frac{\hbar}{m}\mathbf{k}\cdot\mathbf{p}\right]u_{n,\mathbf{k}}(\mathbf{r}) = \epsilon_{n,\mathbf{k}}u_{n,\mathbf{k}}(\mathbf{r}), \tag{4}$$

where $\epsilon_{n,\mathbf{k}} \equiv E_{n,\mathbf{k}} - \frac{\hbar^2k^2}{2m}$. Expanding the above Hamiltonian at given high symmetry point $\mathbf{k}_0$, the eigen-equation at $\mathbf{k}_0+\mathbf{k}$ can be obtained by

$$\left[H_{\mathbf{k}_0} + \frac{\hbar}{m}\mathbf{k}\cdot\mathbf{P}\right]u_{n,\mathbf{k}_0+\mathbf{k}}(\mathbf{r}) = \epsilon_{n,\mathbf{k}_0+\mathbf{k}}u_{n,\mathbf{k}_0+\mathbf{k}}(\mathbf{r}), \tag{5}$$

where $\mathbf{P} = \mathbf{p} + \frac{\hbar}{4m^2c^2}(\sigma\times\nabla V)$. Once $E_{n,\mathbf{k}_0}$ and $u_{n,\mathbf{k}_0}$ are known, the function $u_{n,\mathbf{k}_0+\mathbf{k}}(\mathbf{r})$ can be obtained by treating the term $H_{kp} = \frac{\hbar}{m}\mathbf{k}\cdot\mathbf{P}$ in equation (5) as a perturbation. It is more convenient to rewrite the perturbation term as

$$H_{kp} = \frac{\hbar}{m}\mathbf{k}\cdot\mathbf{P} = \frac{\hbar}{2m}\left(k_+P_- + k_-P_+\right) + \frac{\hbar}{m}k_zP_z, \tag{6}$$

where the operator $P_\pm = P_x \pm iP_y$ and $k_\pm = k_x \pm ik_y$.

From the first-principles calculation results of the SmB_6 system, we find that there are four double degenerate states near the Fermi energy around the X point. Three of them are Sm 4f bands with total angular momentum j = 5/2, the other one is the inverted Sm 5d band. Along Γ-X, the little group is C_{4v}. According to the orbital component analysis of the LDA wave function at the X point, the main components of the inverted Sm 5 d band are $|3/2, \pm3/2\rangle$ ($j^2 = (3/2+1)3/2$, $j_z = \pm3/2$ state), $|5/2, \pm3/2\rangle$ and $|5/2, \pm5/2\rangle$ states. From the symmetry point of view, they behave exactly the same under C_{4v}, since the rotation symmetry is discrete, the only good quantum number j_z is 'conserved' up to a value module 4. For example, under C_4 operation, which can be written as $\hat{C}_{4z} = e^{-i\frac{2\pi}{4}\hat{j}_z}$, states with $j_z = -5/2$ behave exactly the same as $j_z = 3/2$, and states with $j_z = 5/2$ behave exactly the same as $j_z = -3/2$. Therefore we label the inverted Sm 5d states along the Γ-X direction as $|j_z = \pm3/2\rangle$ for simplicity. We emphasize that the 'j_z' quantum numbers discussed throughout the rest of the paper are all defined in this sense. Therefore, we can project the k·p Hamiltonian equation (6) into the following basis at the X point.

$$\left|j_z=\frac{3}{2}\right\rangle_d,\ \left|j_z=-\frac{3}{2}\right\rangle_d,\ \left|j_z=\frac{5}{2}\right\rangle_f,\ \left|j_z=-\frac{5}{2}\right\rangle_f,$$
$$\left|j_z=\frac{3}{2}\right\rangle_f,\ \left|j_z=-\frac{3}{2}\right\rangle_f,\ \left|j_z=\frac{1}{2}\right\rangle_f,\ \left|j_z=-\frac{1}{2}\right\rangle_f. \tag{7}$$

The symmetry-allowed matrix elements of H_{kp} are determined by the symmetry group at X point, which is the D_{4h} group and contains the following symmetries:

(i) fourfold rotation along the z direction $\hat{C}_{4z}=\mathrm{e}^{-\mathrm{i}\frac{2\pi}{4}\hat{J}_z}$, where $\hat{J}_\alpha$ ($\alpha=x, y, z$) is the operator for the α component of the total angular momentum.

(ii) inversion symmetry $\hat{P}=I_2\oplus -I_6$, where I_m is the m × m identity matrix.

(iii) time reversal symmetry $\hat{T}=\Theta K=\mathrm{e}^{-\mathrm{i}\pi\hat{J}_y}K$, where K is the complex conjugate operator.

(iv) twofold rotation along the y direction $\hat{C}_{2y}=\mathrm{e}^{-\mathrm{i}\pi\hat{J}_y}$.

The symmetry operations can help us to reduce the number of independent parameters that appear in the k · p Hamiltonian. For example, considering the C_{4z} symmetry, we have

$${}_d\left\langle\frac{3}{2},\frac{3}{2}\right|P_-\left|\frac{5}{2},\frac{5}{2}\right\rangle_f={}_d\left\langle\frac{3}{2},\frac{3}{2}\right|C_{4z}^\dagger C_{4z}P_-C_{4z}^\dagger C_{4z}\left|\frac{5}{2},\frac{5}{2}\right\rangle_f. \tag{8}$$

Since ${}_d\langle\frac{3}{2},\frac{3}{2}|C_{4z}^\dagger={}_d\langle\frac{3}{2},\frac{3}{2}|\mathrm{e}^{\mathrm{i}\frac{2\pi}{4}\frac{3}{2}}$, $C_{4z}P_\pm C_{4z}^\dagger=\mathrm{e}^{\mp\mathrm{i}\frac{2\pi}{4}}P_\pm$ and $C_{4z}|\frac{5}{2},\frac{5}{2}\rangle_f=\mathrm{e}^{-\mathrm{i}\frac{2\pi}{4}\frac{5}{2}}|\frac{5}{2},\frac{5}{2}\rangle_f$, we get that $c_1\equiv\frac{\hbar}{2m}{}_d\langle\frac{3}{2},\frac{3}{2}|P_-|\frac{5}{2},\frac{5}{2}\rangle_f$ is invariant under C_{4z} rotation and can be non-zero, while ${}_d\langle\frac{3}{2},\frac{3}{2}|P_+|\frac{5}{2},\frac{5}{2}\rangle_f$ gets a minus sign under C_{4z} rotation, which means it must vanish. Following the same procedure, we get $c_1'\equiv\frac{\hbar}{2m}{}_d\langle\frac{3}{2},-\frac{3}{2}|P_+|\frac{5}{2},-\frac{5}{2}\rangle_f$ is finite. We further consider the C_{2y} symmetry and get the relation between c_1 and c_1' as

$$\begin{aligned}c_1&=\frac{\hbar}{2m}{}_d\left\langle\frac{3}{2},\frac{3}{2}\right|P_-\left|\frac{5}{2},\frac{5}{2}\right\rangle_f=\frac{\hbar}{2m}{}_d\left\langle\frac{3}{2},\frac{3}{2}\right|C_{2y}^\dagger C_{2y}P_-C_{2y}^\dagger C_{2y}\left|\frac{5}{2},\frac{5}{2}\right\rangle_f\\&=-\frac{\hbar}{2m}{}_d\left\langle\frac{3}{2},-\frac{3}{2}\right|P_+\left|\frac{5}{2},-\frac{5}{2}\right\rangle_f=-c_1'.\end{aligned} \tag{9}$$

Due to time-reversal symmetry, c_1 can be chosen to be real. Similar considerations can be used to calculate all matrix elements. Finally the effective Hamiltonian which is invariant under all symmetry operations at the X point must have the following form,

$$H_X=\begin{pmatrix}\epsilon_d & 0 & c_1k_+ & c_2k_z & c_3k_z & c_4k_+ & c_5k_- & 0\\ & \epsilon_d & c_2k_z & -c_1k_- & -c_4k_- & c_3k_z & 0 & -c_5k_+\\ & & \epsilon_{f_5} & 0 & 0 & d_1 & 0 & 0\\ & & & \epsilon_{f_5} & d_1 & 0 & 0 & 0\\ & & & & \epsilon_{f_3} & 0 & 0 & 0\\ & & \dagger & & & \epsilon_{f_3} & 0 & 0\\ & & & & & & \epsilon_{f_1} & 0\\ & & & & & & & \epsilon_{f_1}\end{pmatrix}, \tag{10}$$

where $\epsilon_d=D+D_{xy}(k_x^2+k_y^2)+D_zk_z^2$, $\epsilon_{f_i}=F_i+F_{i,xy}(k_x^2+k_y^2)+F_{i,z}k_z^2$ ($i=5, 3, 1$) and $k_\pm=k_x\pm ik_y$. The fitted parameters are listed in table 1 and the energy dispersions are shown in figure 2. It shows that our model Hamiltonian with eight bands captures the main features of the band dispersion near X point.

3.2. Model Hamiltonians for surface states

An important physical consequence of the non-trivial topological band structure is the existence of Dirac-like surface states with helical spin texture. The X points in the bulk BZ are projected to $\bar{\Gamma}$ and $\bar{\mathrm{X}}$ points in the (001) surface BZ as shown in figure 1(b). To study the surface states and the spin texture near $\bar{\Gamma}$ point, we consider a thick slab limited in $z\in[-d/2, d/2]$ with open boundary conditions, where d is the thickness of the slab in z direction. Then k_z is not a good quantum number which should be replaced by $-\mathrm{i}\partial_z$. The eigen wave function will be given by $\psi(k_x, k_y, z)$, which can be expanded using basis $\{\varphi_n(z)=\sqrt{2/d}\ sin\ [n\pi(z+\frac{d}{2})/d]\}$ ($n=0, 1, 2, 3, \ldots$). The Hamiltonian for the slab structure can be obtained by expanding H_X in basis $\varphi_n(z)$,

Table 1. Parameters in our model Hamiltonian fitted for SmB_6, where the unit of energy is eV and the unit of length is the lattice constant.

D	D_{xy}	D_z	F_1	$F_{1,xy}$	$F_{1,z}$
−1.5698	29.9233	18.2502	−0.0502	−0.0020	−0.0300
F_3	$F_{3,xy}$	$F_{3,z}$	F_5	$F_{5,xy}$	$F_{5,z}$
0.0193	−0.5776	−0.4476	−0.0134	−0.0532	−0.2152
c_1	c_2	c_3	c_4	c_5	d_1
−0.2787	−0.318	−0.502	−0.5066	0.0021	−0.0132

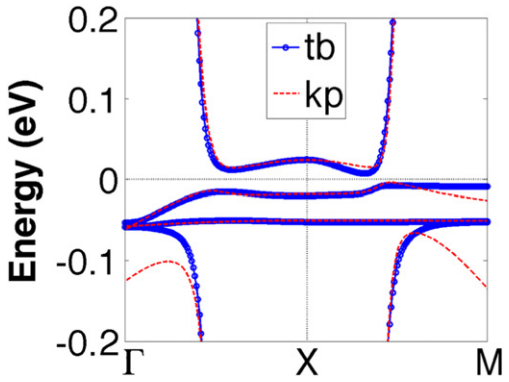

Figure 2. The energy dispersion obtained from our model Hamiltonian (thin red line) is compared with that from tight-binding calculations (thick blue line).

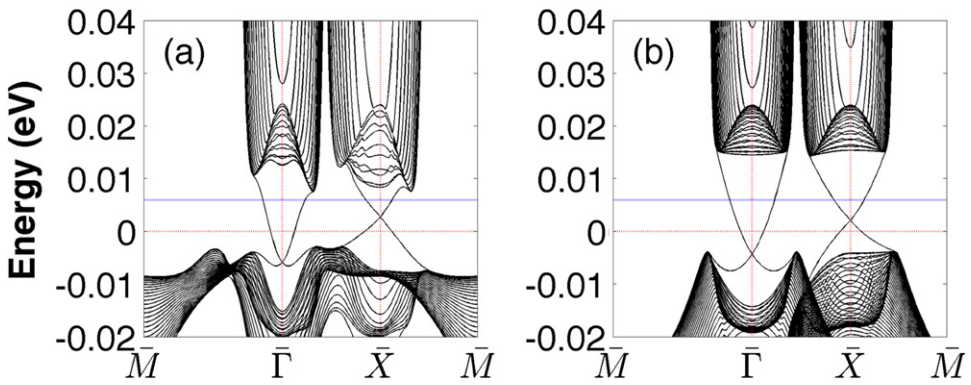

Figure 3. The (001) direction surface states near $\bar{\Gamma}$ and $\bar{\mathrm{X}}$ point, (a) from the tight-binding model; (b) from the k·p model. The blue solid line indicates the energy for the spin-texture calculations.

which is written as $H^{slab}_{\bar{\Gamma},mn}(k_x, k_y) = \langle \varphi_m(z)|H_X(k_x, k_y, -\mathrm{i}\partial_z)|\varphi_n(z)\rangle$ and the surface states near $\bar{\Gamma}$ point can be calculated directly from $H^{slab}_{\bar{\Gamma}}(k_x, k_y)$. For surface states near the $\bar{\mathrm{X}}$ point, we can use the same method but change the z to the x direction. The calculated surface states near $\bar{\Gamma}$ and $\bar{\mathrm{X}}$ points are shown in figure 3(b) and compared with the results from tight-binding calculations in figure 3(a). There are three Dirac cone-like surface states: one located at $\bar{\Gamma}$ points, the other two located at two $\bar{\mathrm{X}}$ points, which is different from most of the known 3D topological insulators, such as Bi_2Se_3.

From $H^{slab}_{\bar{\Gamma},\bar{\mathrm{X}}}$ we can further obtain the spin texture of the surface states near $\bar{\Gamma}$ and $\bar{\mathrm{X}}$ points. The spin texture at the energy of 6 meV is shown in figure 4, which shows a strong spin-momentum locked configuration on the surface states. For a better understanding of the spin textures on the surface states, we construct the surface model Hamiltonians at $\bar{\Gamma}$ and $\bar{\mathrm{X}}$ points on the 2D projected surface BZ. On the 2D BZ, the symmetry group is C_{4v} at $\bar{\Gamma}$ and C_{2v} at $\bar{\mathrm{X}}$. Using the same method as discussed earlier, we can write down the effective Hamiltonians for the surface states at $\bar{\Gamma}$ and $\bar{\mathrm{X}}$ points respectively:

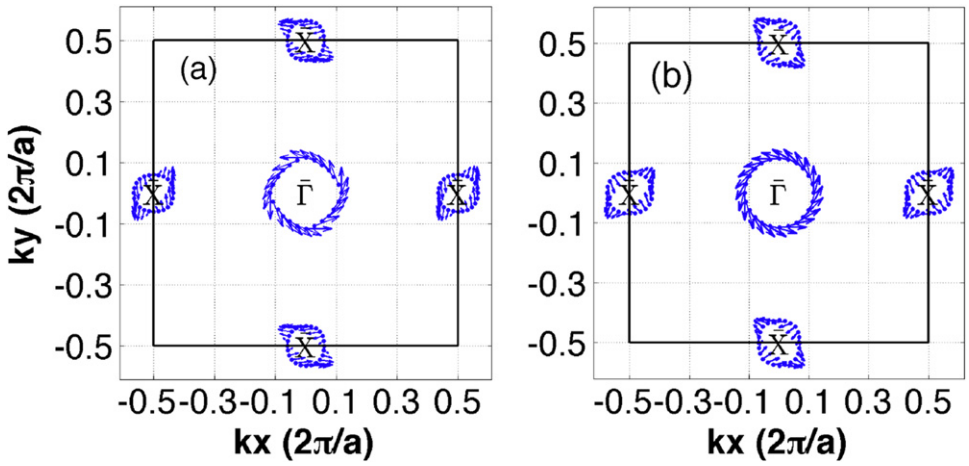

Figure 4. Spin texture on the (001) direction surface states near the $\bar{\Gamma}$ and $\bar{X}$ point, (a) for the tight-binding model results; (b) for the k·p model results.

Table 2. Parameters for the surface states model. The unit of energy is eV and the unit of length is the lattice constant.

$H^{ss}_{\bar{\Gamma}}$	c_0	c_1	c_2	c_3
	0.64105	0.01524	1.1081	−0.0516
	ϵ_0	g_{xx}	g_{yy}	g_{zz}
	−0.0058	−0.5695	0.5695	−0.4768
$H^{ss}_{\bar{X}}$	a_0	a_1	a_2	ϵ_1
	0.011276	0.003059	−0.02322	0.0028
	g_{xx}	g_{yy}	g_{zz}	
	−0.3514	0.6647	0.7825	

1) At the $\bar{\Gamma}$ point: we first discuss the basis functions used for the model Hamiltonian near the $\bar{\Gamma}$ point. The C_4 symmetry in the little group at the $\bar{\Gamma}$ point requires that the eigenstates must also be the eigenstates of the C_4 operator and the time reversal symmetry forces them to form Kramers pairs. From group theory we know that there are two kinds of two-dimensional irreducible representations for the double group of C_{4v}, which are the $|\pm 1/2\rangle$ representation and $|\pm 3/2\rangle$ representation respectively. Again the j_z number mentioned here is defined mod 4, as explained previously. The symmetry analysis for the surface states of SmB_6 obtained by our tight-binding model show that the Dirac surface states at $\bar{\Gamma}$ belong to the representation of $j_z = \pm 3/2$. Therefore the Hamiltonian satisfied the C_{4v} and time-reversal symmetry must have the following form up to the third order of k

$$H^{ss}_{\bar{\Gamma}}(k) = \left(\epsilon_0 + c_0 k^2\right) + \left[\mathrm{i}\left(c_1 k_+ + c_2 k_+^2 k_- + c_3 k_-^3\right)\hat{\sigma}_+ + \mathrm{h.c.}\right] \tag{11}$$

in the basis of $\{|j_z = 3/2\rangle, |j_z = -3/2\rangle\}$. Here $\hat{\sigma}_\pm = \hat{\sigma}_x \pm \mathrm{i}\hat{\sigma}_y, k_\pm = k_x \pm \mathrm{i}k_y$ and $k^2 = k_x^2 + k_y^2$. In equation (11) we keep two k third-order terms in order to fit the nonlinear dispersion band structure better. The parameters in equation (11) are listed in table 2.

To calculate the spin texture of the surface states, we should determine the spin operators $\hat{s}_{x,y,z}$ for the surface Hamiltonian in equation (11) first. We start from the tight-binding Hamiltonian H_{eff}, which is written in the tight-binding basis space expanded by d and f orbitals located at Sm atoms. Based on this tight-binding model we can construct a thick slab terminated in the (001) direction and calculate the surface states $|\Psi_\alpha\rangle, \alpha = 1, 2$. The spin operator $\hat{\mathbf{S}}$ for this slab system can be easily written in the tight-binding basis. Then, we project the spin operator $\hat{\mathbf{S}}$ into the surface states subspace $|\Psi_\alpha\rangle$. Finally, we find that the spin operators for surface states are

$$s_x^{\alpha\beta} = \langle \Psi_\alpha | \hat{S}_x | \Psi_\beta \rangle = 0.0953\sigma_x^{\alpha\beta},$$
$$s_y^{\alpha\beta} = \langle \Psi_\alpha | \hat{S}_y | \Psi_\beta \rangle = -0.0953\sigma_y^{\alpha\beta},$$
$$s_z^{\alpha\beta} = \langle \Psi_\alpha | \hat{S}_z | \Psi_\beta \rangle = 0.0638\sigma_z^{\alpha\beta}. \quad (12)$$

The total angular momentum operators in the surface states subspace also be calculated as $\hat{j}_x = -0.6648\hat{\sigma}_x$, $\hat{j}_y = 0.6648\hat{\sigma}_y$, $\hat{j}_z = -0.5405\hat{\sigma}_z$. With equations (11) and (12), the spin texture of the surface states at $\bar{\Gamma}$ point can be calculated as

$$\langle \mathbf{s} \rangle_{\bar{\Gamma}} \propto \eta \left[-k_y \left(A + Bk_x^2 + Ck_y^2 \right),\ k_x \left(A + Bk_y^2 + Ck_x^2 \right),\ 0 \right] \quad (13)$$

where $A = c_1, B = c_2 - 3c_3, C = c_2 + c_3$ and $\eta = \pm 1$ indicates the energies above and below the Dirac point.

In order to predict or understand properties of the surface states under the external magnetic field, we write down the Zeeman coupling terms for surface states, which takes the following form

$$H_{\bar{\Gamma}}^{ss,Z} = \mu_B \sum_{\alpha,\beta} g_{\alpha\beta} \hat{\sigma}_\alpha B_\beta, \quad (14)$$

which is obtained by projecting the $H_{\text{Zeeman}} = \frac{\mu_B}{\hbar}(\hat{\mathbf{L}} + 2\hat{\mathbf{S}}) \cdot \mathbf{B}$ term into the surface states subspace. Here $\hat{\mathbf{L}}$ and $\hat{\mathbf{S}}$ are the orbital angular momentum and spin operators of the slab system. The non-zero matrix elements of the g factor matrix for surface states at the $\bar{\Gamma}$ point are listed in table 2.

2) At the $\bar{\text{X}}$ point: as shown in figure (3), the Dirac cone near the $\bar{\text{X}}$ point has a good linear dispersion. The surface effective Hamiltonian which satisfies the C_{2v} and time-reversal symmetry can be written in the following form up to the second order of k

$$H_{\bar{X}}^{ss}(\mathbf{k}) = \left(\epsilon_1 + a_0 k^2 \right) + \left[\mathrm{i} \left(a_1 k_+ + a_2 k_- \right) \hat{\sigma}_+ + \text{h.c.} \right] \quad (15)$$

in the basis of $\{|j_z = \frac{3}{2}\rangle, |j_z = -\frac{3}{2}\rangle\}$. The spin operators for surface states are

$$\hat{s}_x = 0.0687\hat{\sigma}_x;\ \ \hat{s}_y = -0.1223\hat{\sigma}_y;\ \ \hat{s}_z = -0.1484\hat{\sigma}_z. \quad (16)$$

The spin texture at the $\bar{X}$ point has the form

$$\langle \mathbf{s} \rangle_{\bar{X}} \propto \eta \left[k_y (a_2 - a_1),\ k_x \left(a_2 + a_1 \right),\ 0 \right]. \quad (17)$$

Both C_{2z} and TRS transform a state from k to −k. C_{2z} symmetry requires $\langle s_z \rangle$ to have the same value at the k and −k points, but TRS requires $\langle s_z \rangle$ to have opposite values at the k and −k points, and so $\langle s_z \rangle$ must be zero as shown in equations (17) and (13), The total angular momentum operators in the surface states subspace can also be calculated as $\hat{j}_x = -0.4201\hat{\sigma}_x, \hat{j}_y = 0.7870\hat{\sigma}_y\ \hat{j}_z = 0.9309\hat{\sigma}_z$. The Zeeman term for surface states at the $\bar{\text{X}}$ point is the same as equation (14) and the g factors are listed in table 2. The spin texture in figure 4 can be well reproduced by our surface states model Hamiltonian. To calculate the surface states spin texture, one must pay attention to the fact that the Pauli matrices in equations (11) and (15) are pseudo-spin operators. The relations between the real and pseudo spin operators are given in equations (12) and(16). These results are different to the cases of the Bi_2Se_3 family of materials. As discussed previously, for a k-point with point group C_{4v} or C_{3v}, the only two possible representations are $j_z = \pm 1/2$ and $j_z = \pm 3/2$. The surface states at $\bar{\Gamma}$ of Bi_2Se_3 belong to the former and those of SmB_6 belong to the latter, leading to different behavior of the g-factor as discussed above.

4. Quasi-particle interference on the SmB_6 (111) surface

In this section we study the quasi-particle interference (QPI) for the surface states, which is important for exploring and understanding many properties of the band structure and can be measured by a Fourier-transform scanning tunneling spectroscopy (FT-STS) experiment. The FT-STS technique is a powerful tool that takes advantage of impurity scattering, which leads to QPI patterns in the density of states on a surface. STS experiments measure the local density of states (LDOS) $\rho(\mathbf{r}, \omega)$ at real-space $\mathbf{r}$ and at energy ω. Then by a Fourier transform of this LDOS one can access the interference pattern $\rho(\mathbf{q}, \omega)$ in momentum space $\mathbf{q}$, which contains useful information about the Fermi surface structure. The principle for the QPI is that the impurity scattering will mix two quasi-particle eigenstates with momenta $\mathbf{k}_1$ and $\mathbf{k}_2$ on a contour of constant energy in the Brillouin zone. The resulting interference at wave $\mathbf{q} = \mathbf{k}_2 - \mathbf{k}_1$ reveals a modulation of the LDOS. Theoretically we can use the exact formulation of the T-matrix to calculate $\rho(\mathbf{q}, \omega)$ associated with any type of impurity [48–51]. In this section we first give the formula to calculate the QPI, then we present the numerical results for

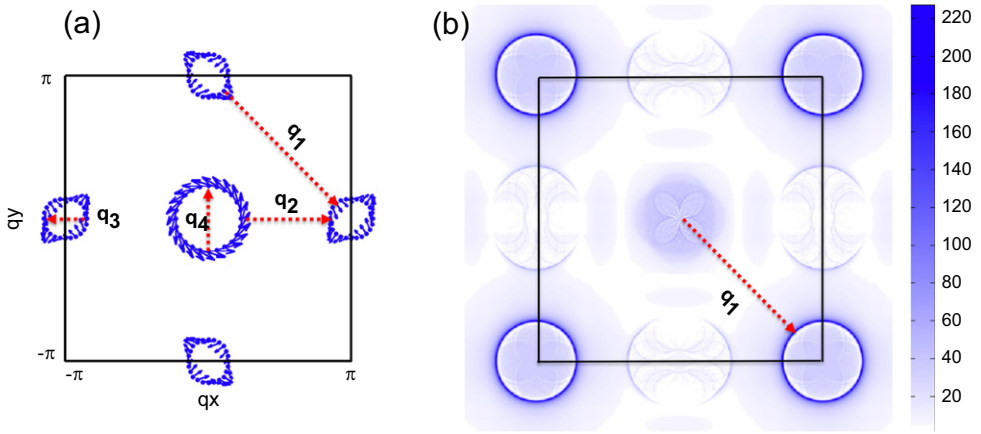

Figure 5. Calculated spin-texture and QPI patterns on SmB_6 (001) surface. (a) The spin texture of the surface states at $\omega = 6$ meV. (b) The QPI patterns $|\rho(\mathbf{q}, \omega)|$. The color in (b) indicates the intensity of the QPI signal.

the QPI on the SmB_6 (001) surface calculated with the effective Hamiltonians equations (11) and (15) constructed in section 3.2.

Formula: we consider a Hamiltonian can be separated into an unperturbed part H_0 and an impurity scattering part H_{imp}: $H = H_0 + H_{\text{imp}}$. The Green's function in the presence of N impurities can be solved by the T-matrix formula [52, 53]

$$G(\mathbf{r}, \mathbf{r}', \omega) = G_0(\mathbf{r}, \mathbf{r}', \omega) + \sum_{i,j=1}^{N} G_0(\mathbf{r}, \mathbf{r}_i, \omega) T(\mathbf{r}_i, \mathbf{r}_j, \omega) G_0\left(\mathbf{r}_j, \mathbf{r}', \omega\right), \tag{18}$$

where the T matrix is defined as

$$T(\mathbf{r}_i, \mathbf{r}_j, \omega) = H_{\text{imp}}(\mathbf{r}_i)\delta_{\mathbf{r}_i,\mathbf{r}_j} + H_{\text{imp}}(\mathbf{r}_i) \sum_{i'=1}^{N} G_0(\mathbf{r}_i, \mathbf{r}_{i'}, \omega) T(\mathbf{r}_{i'}, \mathbf{r}_j, \omega), \tag{19}$$

where $\mathbf{r}_i, \mathbf{r}_j$ and $\mathbf{r}_{i'}$ are the impurity location. The Green's function $G_0(\omega)$ corresponds to unperturbed Hamiltonian $H_0(\mathbf{k})$ which reads $G_0(\mathbf{k}, \omega) = \left(\omega + i\eta - H_0(\mathbf{k})\right)^{-1}$ in the momentum space. We consider a single non-magnetic point-like impurity located at the origin $\mathbf{r} = 0$ in real space: $H_{\text{imp}} = V_0\delta(\mathbf{r})\sigma_0$, where V_0 represents the scattering strength for a non-magnetic impurity, σ_0 is a 2×2 identity matrix. Taking advantage of the translational symmetry of the clean system and momentum independence of the scattering potential, the T-matrix in equation (19) can be simplified as

$$T(\omega) = V(I - g(\omega)V)^{-1}, \tag{20}$$

where $g(\omega) = \sum_k G_0(\mathbf{k}, \omega)/N_i$, N_i is the total number of sites on the surface. The LDOS is give by $\rho(\mathbf{r}, \omega) = -Im\ tr\ [G(\mathbf{r}, \mathbf{r}, \omega)]/\pi$. The QPI is characterized by the Fourier-transform of the LDOS, that is

$$\rho(\mathbf{q}, \omega) = \sum_r \rho(\mathbf{r}, \omega) e^{-i\mathbf{q}\cdot\mathbf{r}} = -\frac{1}{2\pi i} Tr\left[A(\mathbf{q}, \omega) - A^{\star}(-\mathbf{q}, \omega)\right], \tag{21}$$

where the spectral function $A(\mathbf{q}, \omega) \equiv \frac{1}{N_i}\Sigma_{\mathbf{k}} G_0(\mathbf{k} + \mathbf{q}, \omega) T(\omega) G_0(\mathbf{k}, \omega)$, and we have ignored the term $Tr\ [G_0(\mathbf{k}, \omega)]$ in equation (21), which only contributes to the uniform part of DOS. Below we show the QPI $\rho(\mathbf{q}, \omega)$ on the SmB_6 (001) surface calculated by using above formulas.

Numerical results: as shown in figure 5(a), there are four types of possible scattering process on the iso-energy contour of surface states, which connect different parts of the Fermi surfaces and are represented as $q_{1,2,3,4}$. After considering the spin-texture on the surface states, only the first type of scattering is prominent, which is between two Fermi pockets around the $\bar{X}$ points. All other types of scattering processes are greatly suppressed as shown in figure 5(b), which can be understood by the following. The scattering processes associated with vectors q_3 and q_4 are suppressed, because during these processes an electron around the Fermi surface with momenta k will be scattered to its time reversal state with opposite spin direction, which is impossible for non-magnetic impurities. Although the two states connected by vector q_2 are not time reversal partners, their spin directions are almost opposite to each other as shown in figure 5(a), therefore the scattering precesses associated with vector q_2 are also

suppressed. However for the scattering between two pockets around $\bar{X}$, which is associated with with vector q_1, the initial and final states have almost parallel spin direction leading to a ring like feature around the (π,π) points in the QPI pattern.

5. Summary

To summarize, we have derived the model Hamiltonians around three X points for the 3D TI SmB_6 based on the first principles results and the symmetry considerations. The bulk band structure, the surface states and the spin texture in the (001) direction surface can be described well by our model Hamiltonians. We calculated the quasi-particle interference patterns on the (001) surface by using our surface model Hamiltonians. These effective Hamiltonians could facilitate further investigations of this material.

Acknowledgments

This work was supported by the WPI Initiative on Materials Nanoarchitectonics, and Grant-in-Aid for Scientific Research under the Innovative Area 'Topological Quantum Phenomena' (no. 25103723), MEXT of Japan. HMW, ZF and XD acknowledge the NSF of China and the 973 Program of China (no. 2011CBA00108 and no. 2013CB921700) for support.

Note added in proof.
Upon finalizing the manuscript we noticed two recent works on surface states model Hamiltonians and spin texture on the SmB_6 system [54, 55]. The surface model Hamiltonians obtained in [54] are differernt with ours simply because they used different basis functions. If we rotate the axis in pseudo spin space by $\pi/2$ clockwise in our model Hamiltonians (equations (11) and (15)), $\sigma_y \rightarrow \sigma_x$ and $\sigma_x \rightarrow -\sigma_y$, we get formulas the same as theirs.

References

[1] Qi X L and Zhang S C 2011 *Rev. Mod. Phys.* **83** 1057–110
[2] Hasan M Z and Kane C L 2010 *Rev. Mod. Phys.* **82** 3045–67
[3] Roushan P, Seo J, Parker C V, Hor Y S, Hsieh D, Qian D, Richardella A, Hasan M Z, Cava R J and Yazdani A 2009 *Nature* **460** 1106–9
[4] Alpichshev Z, Analytis J G, Chu J H, Fisher I R, Chen Y L, Shen Z X, Fang A and Kapitulnik A 2010 *Phys. Rev. Lett.* **104** 016401
[5] Zhang T *et al* 2009 *Phys. Rev. Lett.* **103** 266803
[6] Xia Y *et al* 2009 *Nat. Phys.* **5** 398–402
[7] Beidenkopf H, Roushan P, Seo J, Gorman L, Drozdov I, Hor Y S, Cava R J and Yazdani A 2011 *Nat. Phys.* **7** 939–43
[8] Fu L and Kane C L 2008 *Phys. Rev. Lett.* **100** 096407
[9] Santos L, Neupert T, Chamon C and Mudry C 2010 *Phys. Rev.* B **81** 184502
[10] Qi X L, Hughes T L and Zhang S C 2010 *Phys. Rev.* B **82** 184516
[11] Moore J E 2010 *Nature* **464** 194–8
[12] Dzero M, Sun K, Galitski V and Coleman P 2010 *Phys. Rev. Lett.* **104** 106408
[13] Takimoto T 2011 *J. Phys. Soc. Jpn.* **80** 123710
[14] Dzero M, Sun K, Coleman P and Galitski V 2012 *Phys. Rev.* B **85** 045130
[15] Alexandrov V, Dzero M and Coleman P 2013 *Phys. Rev. Lett.* **111** 226403
[16] Ye M, Allen J W and Sun K 2013 arXiv:1307.7191
[17] Dzero M and Galitski V 2013 *J. Exp. Theor. Phys.* **117** 499–507
[18] Lu F, Zhao J, Weng H, Fang Z and Dai X 2013 *Phys. Rev. Lett.* **110** 096401
[19] Weng H, Zhao J, Wang Z, Fang Z and Dai X 2014 *Phys. Rev. Lett.* **112** 016403
[20] Deng X, Haule K and Kotliar G 2013 *Phys. Rev. Lett.* **111** 176404
[21] Alexandrov V, Dzero M and Coleman P 2013 *Phys. Rev. Lett.* **111** 226403
[22] Legner M, Ruegg A and Sigrist M 2014 *Phys. Rev.* B **89** 085110
[23] Werner J and Assaad F F 2013 *Phys. Rev.* B **88** 035113
[24] Frantzeskakis E *et al* 2013 *Phys. Rev.* X **3** 041024
[25] Wolgast S, Kurdak Ç, Sun K, Allen J W, Kim D J and Fisk Z 2013 *Phys. Rev.* B **88** 180405
[26] Xu N *et al* 2013 *Phys. Rev.* B **88** 121102
[27] Li G *et al* 2013 arXiv:1306.5221
[28] Neupane M *et al* 2013 *Nat. Commun.* **4** 3786
[29] Kim D J, Thomas S, Grant T, Botimer J, Fisk Z and Xia J 2013 *Nature Scientific Reports* **3** 3150
[30] Jiang J *et al* 2013 *Nat. Commun.* **4** 3010
[31] Thomas S, Kim D J, Chung S B, Grant T, Fisk Z and Xia J 2013 arXiv:1307.4133
[32] Yee M M, He Y, Soumyanarayanan A, Kim D J, Fisk Z and Hoffman J E 2013 arXiv:1308.1085
[33] Denlinger J D, Allen J W, Kang J S, Sun K, Kim J W, Shim J H, Min B I, Kim D J and Fisk Z 2013 arXiv:1312.6637
[34] Frantzeskakis E *et al* 2013 *Phys. Rev.* X **3** 041024
[35] Ruan W, Ye C, Guo M, Chen F, Chen X, Zhang G M and Wang Y 2014 *Phys. Rev. Lett.* **112** 136401
[36] Denlinger J D *et al* 2014 *JPS Conf. Proc.* **3** 017038
[37] Beaurepaire E, Kappler J P and Krill G 1990 *Phys. Rev.* B **41** 6768–76
[38] Cohen R L, Eibschutz M and West K W 1970 *Phys. Rev. Lett.* **24** 383–6

[39] Eibschutz M, Cohen R L, Buehler E and Wernick J H 1972 *Phys. Rev.* B **6** 18–23
[40] Chazalviel J N, Campagna M, Wertheim G K and Schmidt P H 1976 *Phys. Rev.* B **14** 4586–92
[41] Kane C L and Mele E J 2005 *Phys. Rev. Lett.* **95** 146802
[42] Fu L and Kane C 2006 *Phys. Rev.* B **74** 195312
[43] Deng X, Wang L, Dai X and Fang Z 2009 *Phys. Rev.* B **79** 075114
[44] Kotliar G, Savrasov S, Haule K, Oudovenko V, Parcollet O and Marianetti C 2006 *Rev. Mod. Phys.* **78** 865–951
[45] Kune J, Arita R, Wissgott P, Toschi A, Ikeda H and Held K 2010 *Comput. Phys. Commun.* **181** 1888–95
[46] Solovyev I V, Pchelkina Z V and Anisimov V I 2007 *Phys. Rev.* B **75** 045110
[47] Mostofi A A, Yates J R, Lee Y S, Souza I, Vanderbilt D and Marzari N 2008 *Comput. Phys. Commun.* **178** 685–99
[48] Balatsky A, Vekhter I and Zhu J X 2006 *Rev. Mod. Phys.* **78** 373–433
[49] Zhou X, Fang C, Tsai W F and Hu J 2009 *Phys. Rev.* B **80** 245317
[50] Lee W C, Wu C, Arovas D P and Zhang S C 2009 *Phys. Rev.* B **80** 245439
[51] Guo H M and Franz M 2010 *Phys. Rev.* B **81** 041102
[52] Zhou X, Fang C, Tsai W F and Hu J 2009 *Phys. Rev.* B **80** 245317
[53] Morr D K and Stavropoulos N A 2003 *Phys. Rev.* B **67** 020502
[54] Roy B, Sau J D, Dzero M and Galitski V 2014 *Phys. Rev.* B **90** 155314
[55] Baruselli P P and Vojta M 2014 *Phys. Rev.* B **90** 201106